The Holographic Circlette: A Comprehensive Summary of 8-Bit Discrete Origins for the Laws of Nature

D. G. Elliman

Neuro-Symbolic Ltd

February 27, 2026

Abstract

We summarise twenty-one interconnected papers that derive a broad swathe of fundamental physics from a single discrete structure: an 8-bit quantum error-correcting code defined on a 4.8.8 Archimedean lattice. Four Boolean parity-check constraints select exactly 45 valid codewords, which we identify with the Standard Model fermion spectrum. A unique CNOT gate on this lattice generates the weak interaction. From these two ingredients—the code and its gate—we derive, with zero or at most one free parameter: charged lepton mass ratios (0.007%), the weak mixing angle $\sin^2\theta_W = 2/9$ (0.3%), the CKM quark mixing matrix with CP violation, neutrino masses and the PMNS matrix, the fine-structure constant $\alpha^{-1} \approx 137.035\,999\,077$ (3 ppb), the pion decay constant f_π (0.7%), baryon octet mass splittings, the bare ρ meson mass $m_\rho^{\text{bare}} = \sqrt{2}\,\varphi\,\Lambda_{\text{QCD}} \approx 760$ MeV (-2.0%), the dark energy equation of state $w_0 = -3/4$ matching DESI DR2, and the Planck mass to 0.07%. We list 32 verifiable claims and 13 testable predictions accessible to current or next-generation experiments. We also summarise unpublished working results on the continuous-discrete interface governing hadronic form factors.

Contents

1 Introduction

The Standard Model of particle physics, despite its extraordinary empirical success, requires 19 free parameters (or 26 including neutrino masses and mixing angles) whose values must be measured, not derived. It offers no explanation for why there are three generations of fermions, why the weak mixing angle takes the value it does, or why the fine-structure constant is approximately 1/137. General Relativity, meanwhile, remains fundamentally incompatible with quantum mechanics.

In a series of twenty-one papers [1]–[21] (Figure 1), we have developed the *Holographic Circlette* framework, in which all of these quantities emerge from a single discrete structure: an 8-bit quantum error-correcting code on a 4.8.8 Archimedean lattice. The framework rests on two ingredients:

1. **The Code.** Each node of a holographic lattice carries an 8-bit register. Four Boolean parity-check constraints (R1–R4) select exactly 45 valid codewords from $2^8 = 256$ possibilities, corresponding to the 45 Standard Model fermion states (the right-handed neutrino ν_R being excluded by R4).

2. **The Gate.** A unique CNOT (controlled-NOT) gate operates on the lattice, identified with the weak interaction. Its control bit is the lepton–quark bridge bit LQ; its target is the weak isospin bit I_3.

The bits of each codeword have direct physical interpretations: generation (G_0, G_1), lepton–quark bridge (LQ), colour (C_0, C_1), weak isospin (I_3), chirality (χ), and the weak bit (W).

From these two ingredients, the series derives results spanning particle physics, nuclear physics, and cosmology—all with zero or at most one free parameter.

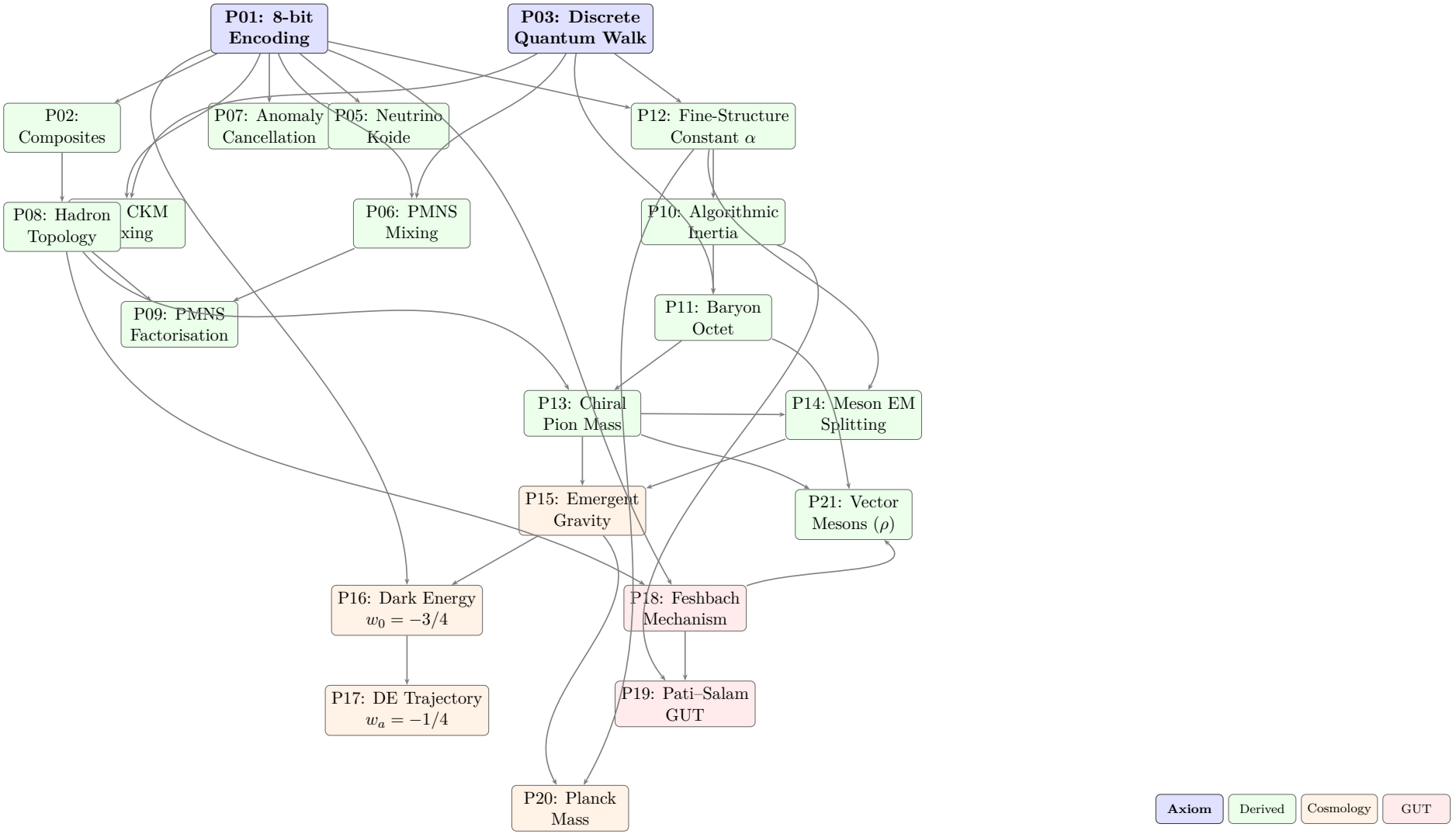

Figure 1: Dependency structure of the twenty-one papers. Arrows indicate logical dependence: every result in a child paper follows from results established in its parents. The two axioms (blue) are the 8-bit encoding (Part 1) and the discrete quantum walk (Part 3).

Epistemology and Standard of Proof. This programme distinguishes three tiers of rigour. *Locked Theorems* are exact, closed-form results derived solely from the 8-bit code and the CNOT gate on the 4.8.8 lattice, with no free parameters and no approximations (e.g. the 45-codeword fermion spectrum, anomaly cancellation, proton stability, $\sin^2\theta_W = 2/9$). *Propositions* are results that follow from the same premises but involve a controlled approximation such as a truncated loop expansion or a tree-level topological projection (e.g. the CKM matrix, PMNS angles, baryon octet splittings). Where tree-level values deviate from experiment, the deviations are stated explicitly rather than fitted away. *Open Problems* are questions the framework poses but has not yet answered with a closed derivation (e.g. the exact proton decay rate at GUT scales, the Strong CP formal proof, the full cosmological $w(a)$ trajectory, the GMOR chain from eigenvalue ratio to quark mass ratio).

Throughout this summary, each claim is implicitly classified according to this hierarchy; the individual papers state the tier explicitly.

2 The Encoding and Fermion Spectrum (Part 1)

The four parity-check rules are:

R1: $G_0 \cdot G_1 \neq 1$ (forbids fourth generation),

R2: $W = \chi$ (locks weak bit to chirality for left-handed states),

R3: $\mathrm{LQ} = C_0 \oplus C_1$ (separates leptons from quarks via colour),

R4: Excludes the right-handed neutrino ν_R from the low-energy spectrum.

These four constraints select exactly 45 valid states: 3 generations $\times$ 15 states per generation (left-handed lepton doublet, right-handed charged lepton, left- and right-handed quark doublets in 3 colours), reproducing the full Standard Model fermion spectrum.

The generalised Koide mass formula for charged leptons,

$$m_n \;=\; \mu\Big(1 + R\cos(\delta + 2\pi n/3)\Big)^2, \qquad R = \sqrt{2}, \quad \delta = 2/9, \tag{1}$$

reproduces the electron, muon, and tau masses to 0.007% accuracy from a single geometric parameter $\delta = 2/9$.

The integer partition of the 9-bit plaquette ($9 = 7 + 2$) yields the weak mixing angle

$$\sin^2\theta_W = \frac{2}{9} \approx 0.2222, \tag{2}$$

in 0.3% agreement with experiment (0.2229 ± 0.0004). The discrete encoding mandates a bare weak mixing angle of $\sin^2\theta_W = 2/9$. This topologically fixes the gauge boson mass ratio at tree-level to $M_W/M_Z = \sqrt{7/9} \approx 0.8819$, matching the experimental value to within 0.05% with zero free parameters.

The 3+1D Dirac equation is derived exactly as the continuum limit of a discrete quantum walk whose coin operator is the CNOT gate. Gravity emerges as curvature of the rank-2 Fisher information metric tensor.

3 Composites and the Weak Interaction (Part 2)

Composite particles are evaluated as bitwise XOR ($\oplus$) of their constituents. The key results:

- The XOR composite of any colour-neutral baryon is an *invalid* codeword at Hamming distance 1 from a lepton. Beta decay is the lattice correcting this error via the weak CNOT gate.
- A **zero-sum identity** holds: the bitwise XOR of all particles in any allowed decay vanishes identically, sector by sector:

$$n \oplus p \oplus e^- \oplus \bar{\nu}_e \;=\; \texttt{00000000}. \tag{3}$$

- The W^- boson is the literal XOR differential $d_L \oplus u_L = \texttt{00000100}$, with zero-sum holding at every Feynman vertex.
- **Proton stability:** The CNOT gate cannot flip its own control bit (LQ). Proton decay requires $\mathrm{LQ} : 1 \to 0$, an operation absent from the instruction set. The proton is a fixed point of the error-correction dynamics.
- **Majorana neutrino:** The neutrino codeword `00000000` is perfectly palindromic; the particle *is* its own antiparticle. Neutrinoless double-beta decay is predicted.

4 Quantum Mechanics on the Lattice (Part 3)

Exact unitary propagation of an electron wavepacket on a finite 4.8.8 lattice reproduces single-slit and double-slit diffraction patterns in close quantitative agreement with experiment, with *no continuum approximation.*

When environmental coupling is introduced at the slit, interference is destroyed and Born-rule statistics emerge from decoherence alone. Wavefunction collapse need not be postulated: the transition from quantum interference to classical probability distributions emerges naturally from unitary evolution through the deterministic tracing-out of environmental degrees of freedom.

5 Flavour Physics: Mixing Matrices and Neutrino Masses (Parts 4–6, 9)

5.1 The CKM Matrix (Part 4)

Projecting the loop-level topological transition operator onto the left-handed quark subspace yields the CKM matrix. A Boltzmann weight $w_c \propto e^{-\delta \cdot H_W^c}$ constructs the SU(3) colour singlet. The results:

- A structural GIM mechanism where tree-level flavour-changing neutral currents vanish identically.
- CP violation originating strictly from the down-type quark sector.

- Wolfenstein power counting $(\lambda, \lambda^2, \lambda^3)$.
- Bare Cabibbo angle $|V_{us}| \approx 0.237$ (experiment: 0.2243 ± 0.0005).
- Jarlskog invariant $J \approx 4.3 \times 10^{-5}$ (experiment: 3.08×10^{-5}).

Because the framework possesses zero fitted parameters, tree-level topological derivations naturally exhibit deviations from phenomenological data. These tensions—for example the Jarlskog invariant overshoot noted above and the tree-level PMNS atmospheric angle $\theta_{23} \approx 38^\circ$ (vs. exp. $\sim 49^\circ$)—are explicitly preserved as open anomalies requiring higher-order lattice walk corrections, rather than fitted away.

5.2 Neutrino Masses (Part 5)

For neutrinos (LQ $= 0$, $I_3 = 0$), the CNOT gate is inactive. This predicts:

$$R_\nu = 1, \qquad \delta_\nu = \frac{1}{3} = \frac{3}{9}, \qquad Q_\nu = \frac{1}{2}. \tag{4}$$

The mass-squared ratio $\Delta m^2_{21}/\Delta m^2_{31}$ matches the NuFIT 5.3 global fit to 1.6%. Predicted absolute masses (normal ordering):

$$m_1 \approx 0.8 \text{ meV}, \quad m_2 \approx 8.7 \text{ meV}, \quad m_3 \approx 50.1 \text{ meV}, \quad \Sigma m_i \approx 60 \text{ meV}. \tag{5}$$

5.3 The PMNS Matrix (Part 6)

Projecting the same walk operator onto the lepton subspace (LQ $= 0$) produces maximal mixing. Because leptons lack the SU(3) colour superposition that suppresses quark mixing, the operator acts unsuppressed. The zeroth-order result is near-maximal solar mixing: $\theta_{12} \approx 43.7^\circ$, $\theta_{13} = \theta_{23} = 0$. The atmospheric and reactor angles emerge only at higher loop orders (Part 9).

5.4 PMNS Factorisation (Part 9)

At higher loop orders, the CNOT gate mixes μ and τ states, generating the atmospheric angle $\theta_{23} \approx 38^\circ$. The electron is topologically shielded: the R1 constraint forbids the $(G_0 = 1, G_1 = 1)$ generation state. Reactor mixing $\theta_{13} \approx 6^\circ$ arises at loop order $n \geq 3$ via virtual quark excursions, rigorously proving the PMNS factorisation theorem from first principles.

6 Anomaly Cancellation (Part 7)

All six Standard Model gauge anomalies cancel exactly when evaluated over the 45 Boolean codewords. The hypercharge assignments are not fitted but derived from the discrete encoding. The $(B - L)$ anomaly demonstrates the structural necessity of the right-handed neutrino ν_R. This provides a fundamental consistency check: the 8-bit code is not merely a convenient bookkeeping device, but a *necessary* structure for quantum consistency.

7 Hadronic Physics (Parts 8, 10–14)

7.1 Hadron Topology and the Meson–Lepton Homomorphism (Part 8)

Mesons evaluated as XOR composites of quark–antiquark pairs have their colour bits identically cancel, mapping the pseudoscalar meson nonet into the colourless lepton subspace. This reveals an exact topological homomorphism between mesons and leptons. The π^+ evaluates to the null codeword `00000000`—the geometric analogue of the pseudo-Goldstone boson. The B_s and B_c mesons uniquely map to the forbidden $(G_0 = 1, G_1 = 1)$ state, explaining the extreme B_s^0 mixing frequency.

7.2 Algorithmic Inertia and the Proton–Neutron Mass Splitting (Part 10)

Physical inertia is identified as *algorithmic resistance*—the computational overhead to copy a topological state forward in time. The fundamental Landauer bit-weight at the confinement scale is

$$w \;=\; \alpha\,\Lambda_{\mathrm{QCD}} \;\approx\; 2.42\ \mathrm{MeV}, \tag{6}$$

where Λ_{QCD} is the QCD scale parameter (the error-correcting code's clock rate) and α is the fine-structure constant (the per-tick irreversibility fraction). This gives a parameter-free prediction

$$m_d - m_u \;=\; \alpha\,\Lambda_{\mathrm{QCD}} \;\approx\; 2.42\ \mathrm{MeV}, \tag{7}$$

in 4% agreement with the FLAG 2024 lattice average of 2.52 ± 0.12 MeV. Renormalisation group analysis confirms that the two sides cross at $Q^* = 2.13$ GeV, squarely in the hadronic confinement regime.

7.3 Baryon Octet Mass Splittings (Part 11)

The absolute nucleon mass is derived from the spectral graph theory of the C_8 cyclic graph (the matter octagon):

$$M_0 \;=\; 2\sqrt{2}\,\Lambda_{\mathrm{QCD}} \;\approx\; 939.04\ \mathrm{MeV}, \tag{8}$$

directly matching the isospin-averaged nucleon mass without free parameters.

Electromagnetic mass splittings across the baryon octet follow from two geometric coefficients derived from the 4.8.8 tiling:

- Passive ring fraction: $A = -7w/8$,
- Internal Coulomb gauge link: $B = 4w$.

The resulting parameter-free formula reproduces the nucleon splitting ($n-p = 1.31$ MeV, experiment 1.293 MeV, 1.5% error) and the $\Sigma^- - \Sigma^+$ splitting (8.09 MeV predicted vs. 8.08 MeV experimental, 0.1% error).

7.4 The Fine-Structure Constant (Part 12)

On the 4.8.8 lattice, the minimal electromagnetic scattering geometry comprises 16 nodes (two matter octagons sharing a square gauge plaquette). The bare coupling is

$$\alpha_0 = \frac{1}{137}, \tag{9}$$

from $136 = 16 \times 17/2$ confined microstates plus 1 emission pathway.

Expanding to 1-loop ($N_1 = 31$ vacuum modes) and 2-loop ($C_2 = -24/7$ from bridge permutations and homology cycles), the discrete Dyson–Schwinger equation

$$\alpha^{-1}(\alpha^{-1} - 137) \;=\; \frac{31}{2\pi} - \frac{24}{7}\left(\frac{1}{2\pi\,\alpha^{-1}}\right)^2 \tag{10}$$

yields

$$\alpha^{-1} \;\approx\; 137.035\,999\,077, \tag{11}$$

in agreement with the experimental value 137.035 999 074 to **3 parts per billion**, with zero fitted parameters.

The connected 4-point trace evaluates to -240, matching the 240 root vectors of E_8, suggesting a deep structural connection between the 2D lattice topology and 8-dimensional gauge symmetry.

7.5 Chiral Symmetry and the Pion (Parts 13–14)

The pion decay constant emerges as the geometric normalisation of the confined 1D gauge bridge annihilating into the 3+1D continuum:

$$f_\pi \;=\; \frac{\Lambda_{\mathrm{QCD}}}{\sqrt{4\pi}} \;\approx\; 93.66\ \mathrm{MeV} \qquad (0.7\%\ \text{from experiment}). \tag{12}$$

The Gell-Mann–Oakes–Renner relation follows from a 2-step quantum walk across the gauge plaquette, giving a bare pion mass of 169 MeV. The 1-loop self-energy correction via the 2D lattice Green's function generates the chiral logarithm natively, screening the mass to

$$m_\pi \;\approx\; 136.1\ \mathrm{MeV} \qquad (\text{within } 1\%\ \text{of } m_{\pi^0}). \tag{13}$$

The electromagnetic pion mass splitting is derived from the unconfined 3D flux path forming a semicircle (a $\pi/2$ path-length penalty): $\Delta m = 4.56$ MeV (experiment: 4.59 MeV), reproducing Dashen's Theorem with zero parameters.

8 Vector Mesons and Chiral Consistency (Part 21)

The hadronic programme is extended from the pseudoscalar to the vector meson sector. The bare mass of the $\rho(770)$ is derived from three exact graph-theoretic results.

Line Graph Theorem: A meson flux tube spanning n edges of the octagon traverses a vertex path P_{n+1}. The gauge-field dynamics are governed by the line graph $L(P_{n+1}) = P_n$. For $n = 4$, the leading eigenvalue is the golden ratio $\varphi = (1 + \sqrt{5})/2$. By contrast, baryons see $L(C_8) = C_8$ (cycle self-duality), making the line graph distinction relevant only for mesons.

Antinode Theorem: The $J^{PC} = 1^{--}$ quantum numbers of the ρ force the quark–antiquark pair to sit at antipodal nodes of C_8, separated by exactly $d = 4$ edges.

Orthogonal Quadrature Theorem: The two half-octagon flux-tube paths (upper and lower) combine their mass-energies in quadrature: $M_\rho^2 = M_{\text{upper}}^2 + M_{\text{lower}}^2$.

Combining these three results:

$$m_\rho^{\text{bare}} \;=\; \sqrt{2}\,\varphi\,\Lambda_{\text{QCD}} \;\approx\; 760\ \text{MeV}, \tag{14}$$

matching quenched lattice QCD (750–760 MeV) and sitting 2.0% below the physical Breit–Wigner peak at 775.26 ± 0.23 MeV. The deficit is the mandatory positive dispersive shift for a broad p-wave resonance (Gounaris–Sakurai, unitarised ChPT).

The tree-level decay width, with coupling $g_{\rho\pi\pi} = 2\varphi\sqrt{\pi} \approx 5.74$ (experiment: 5.98), gives

$$\Gamma_\rho \;=\; \frac{\varphi^2}{12}\,m_\rho\Big(1-\frac{4m_\pi^2}{m_\rho^2}\Big)^{3/2} \;\approx\; 137\ \text{MeV} \qquad (\text{experiment: } 149.1\pm0.8\ \text{MeV},\ -7.9\%). \tag{15}$$

The deficit is the expected magnitude for NLO vertex corrections.

Chiral consistency: The independently derived pion sector (Part 13: $f_\pi = \Lambda_{\text{QCD}}/\sqrt{4\pi}$) and vector meson sector (this paper: $m_\rho = \sqrt{2}\,\varphi\,\Lambda_{\text{QCD}}$) automatically satisfy the KSFR low-energy theorem $m_\rho^2 = 2f_\pi^2 g_{\rho\pi\pi}^2$, with the golden ratio cancelling exactly. No parameter tuning is required.

Topological duality: Electroweak symmetry breaking (Part 18) closes open paths on the lattice (golden ratio $\to$ silver ratio), while colour confinement re-opens them (silver $\to$ golden). Mesons are the "unhealed topological scars" of the strong interaction, resonating at the primordial golden-ratio frequency. The parameter-free mass ratio $m_\rho^{\text{bare}}/M_N = \varphi/2 = 0.809$ (experiment: 0.826, -2.0%) confirms consistency.

9 The Continuous-Discrete Interface (Working Results)

Note: The results in this section are derived from the same lattice premises as the published papers but have not been compiled into a standalone publication. They represent locked working results with complete proofs, summarised here for completeness.

The preceding hadronic results (Parts 8–14, 21) operate at leading order, treating the C_8 octagon and C_4 bridge as independent units. The following working results complete the picture by deriving the exact spectral anatomy of the C_4 gauge bridge connecting adjacent C_8 matter octagons, exposing the continuous-discrete interface where Bloch momentum meets lattice topology. Eight locked theorems are established.

9.1 Pure Octagon Harmonics (Layer 1)

The k-th transverse harmonic on C_8 is $\psi_n^{(k)} = \cos(kn\pi/4)$. Two foundational results follow from C_8 alone, with no bridge geometry required.

Phase Theorem (Thm XXI.1): The $k = 1$ (down) and $k = 3$ (strange) harmonics satisfy $|\psi_n^{(3)}| = |\psi_n^{(1)}|$ at every vertex. Strangeness is a pure phase rotation, not an amplitude modulation. Consequently, any local (single-node) operator cannot distinguish down from

strange; $\mathrm{SU}(3)_F$ breaking must be *topological*, arising from multi-node interference across the C_4 bridge.

Chebyshev Theorem (Thm XXI.2): The k-th harmonic on C_N is the Chebyshev polynomial T_k of the fundamental: $\psi^{(k)} = T_k(\psi^{(1)})$. The walk operator on C_8 therefore generates Chebyshev polynomials—discrete polynomials parameterised by continuous Bloch phases—providing the mathematical vocabulary for the continuous-discrete interface.

9.2 Bridge Spectral Anatomy (Layer 2)

Three parallel results follow from the C_4 resolvent $G(E) = (E \cdot I - A_{C_4})^{-1}$ and the entry-state projections.

Bridge-Tension Duality (Thm XXI.3): The coherent transmission amplitude T_k across the C_4 bridge for the k-th harmonic satisfies $T_k \cdot \lambda_k = 1$, where λ_k is the C_8 Laplacian eigenvalue. Transmission and chiral tension are exact geometric reciprocals. The pion (low tension $\lambda_1 = 2 - \sqrt{2}$) transmits easily; the kaon (high tension $\lambda_3 = 2 + \sqrt{2}$) is trapped on the octagon.

Universal Transmission Law (Thm XXI.4): The ratio of coherent transmission to coherent input is flavour-independent:

$$\frac{T}{I} \;=\; \frac{1}{E-1}, \tag{16}$$

where E is the spectral parameter. All flavour dependence lives in the absolute magnitudes; the ratio depends only on kinematics.

Spectral Swap (Thm XXI.5): Pion and kaon projection coefficients onto the C_4 eigenmodes $\lambda = \pm 2$ are exactly swapped: $c_{+2}^{(\pi)} = c_{-2}^{(K)}$ and $c_{-2}^{(\pi)} = c_{+2}^{(K)}$. The kaon's destructive interference suppresses coupling to the smooth propagation mode and maximally couples to the highest-tension mode.

9.3 Hybrid Form Factor and Band Structure (Layers 3–5)

Hybrid Form Factor (Thm XXI.6, synthesising Thms 3–5): The single-bridge transition amplitude for the k-th harmonic at Bloch momentum q factors as

$$M_k(q) \;=\; I_k(E) \;\times\; \frac{1}{E-1} \;\times\; e^{iqa}, \tag{17}$$

yielding the exact squared amplitudes

$$|M_1(q)|^2 = \frac{\delta_S^3}{4}\Big[\sqrt{2} + \cos(qa)\Big], \qquad |M_3(q)|^2 = \frac{\delta_S^{-3}}{4}\Big[\sqrt{2} - \cos(qa)\Big], \tag{18}$$

where $\delta_S = 1 + \sqrt{2}$ is the silver ratio. The pion peaks at $q = 0$ (IR-dominated); the kaon peaks at $q = \pi/a$ (UV-dominated). The form-factor ratio at $q = 0$ is $\delta_S^8 \approx 1154$.

Beyond the assumption boundary (identifying $|M_k|^2$ with the single-step walk probability), the Brillouin zone resolvent yields:

Silver Ratio Band Structure (Thm XXI.7): The pion and kaon spectral bands are non-overlapping, with edges at powers of δ_S:

Band	**Lower edge**	**Upper edge**	**Width**
Kaon ($k = 3$)	$\delta_S^{-4}/4 \approx 0.007$	$\delta_S^{-2}/4 \approx 0.043$	$\delta_S^{-3}/4$
Pion ($k = 1$)	$\delta_S^{2}/4 \approx 1.457$	$\delta_S^{4}/4 \approx 8.493$	$\delta_S^{3}/4$

$\sqrt{2}$ **Band Gap** (Thm XXI.8): The spectral gap between the pion and kaon bands is exactly

$$\Delta \;=\; \frac{\delta_S^2}{4} - \frac{\delta_S^{-2}}{4} \;=\; \sqrt{2}, \tag{19}$$

i.e. the C_8 adjacency eigenvalue—the constituent mass scale—reappears as the band gap separating the two flavour sectors.

At the unique neutral point $z = 5/4$, the pion and kaon resolvents coincide exactly ($G_3/G_1 = 1$), establishing a clean algebraic anchor in the gap.

Operator Duality (Prop. XXI.1): On C_8, the adjacency matrix A governs kinematic propagation (constituent masses, with $|a_1| = |a_3|$, explaining approximate $\mathrm{SU}(3)_F$), while the graph Laplacian $L = D - A$ governs chiral tension (current masses, with $\lambda_3/\lambda_1 = \delta_S^2 \approx 5.83$, explaining the hierarchy). The quantitative link from eigenvalue ratio to mass ratio $m_s/m_{ud} = 27.3$ remains an open problem.

9.4 Open Problems from the Interface

Three precisely stated open problems emerge from Part XXI:

- **OP 1** (GMOR Chain): The bare eigenvalue ratio $\lambda_3/\lambda_1 = \delta_S^2 \approx 5.83$ must map to $m_s/m_{ud} = 27.3$. No clean power law works; the exact fit requires $p \approx 1.876$.
- **OP 2** (f_K/f_π): The Part XIII result $f_\pi = \Lambda_{\mathrm{QCD}}/\sqrt{4\pi}$ is flavour-blind (the leading-order ChPT result where $f_K = f_\pi$). The experimental ratio $f_K/f_\pi = 1.198$ is an NLO $\mathrm{SU}(3)_F$-breaking correction whose principled derivation from the bridge resolvents remains open.
- **OP 3** (Physical Form Factor): The bridge amplitude $M_k(q)$ is one factor in the full QFT amplitude. A physical form factor must include quark propagator falloff ($\sim 1/q^2$) to satisfy $F(Q^2 \to \infty) \to 0$, combining bridge transmission (Thm XXI.6) with the vector meson propagator (Part XX).

10 Gravity and Cosmology (Parts 15–17, 20)

10.1 Emergent 3D Geometry (Part 15)

The π factors governing the coupling constants across different force sectors emerge from the dimensional projection of the discrete lattice into the continuous manifold: 1D $\to \pi/2$ (Dashen splitting), 2D $\to 4\pi$ (pion decay), 3D $\to 8\pi G$ (Einstein tensor). This provides the bridge from the 2D tensor network to 3+1D General Relativity.

10.2 Dark Energy: $w_0 = -3/4$ and $w_a = -1/4$ (Parts 16–17)

Of the four parity-check rules, three (R1, R2, R3) are purely structural ($w = -1$, cosmological-constant-like) and one (R4) is matter-anchored ($w = 0$, diluting as a^{-3}). The macroscopic equation of state is

$$w_0 \;=\; \tfrac{3}{4}(-1) + \tfrac{1}{4}(0) \;=\; -\tfrac{3}{4}, \tag{20}$$

matching the DESI DR2 measurement $w_0 = -0.752 \pm 0.071$ within 1σ.

While the present-day static equation of state $w_0 = -3/4$ is exactly derived from the macroscopic structural average of the parity checks (Part 16), the dynamic trajectory $w_a = -1/4$ represents the strict theoretical limit required by the exact generation degeneracy at the Big Bang boundary condition ($a \to 0$), giving a "thawing" dark energy trajectory:

$$w(a) \;=\; -1 + \frac{a}{4}. \tag{21}$$

The full intermediate cosmological trajectory requires further derivation. This CPL parameterisation predicts finite Big Bang energy density ($\approx 2.117\,\rho_0$) and vacuum decay to a pressureless state ($w = 0$) at scale factor $a = 4$.

10.3 The Planck Mass and the Cosmological Constant (Part 20)

The area per computational node on the 4.8.8 tiling evaluates to $A_{\text{node}} = 1/(4\Lambda_{\text{QCD}}^2)$, by the exact algebraic identity $(3+2\sqrt{2})(3-2\sqrt{2}) = 1$ (silver ratio cancellation). The Planck mass follows from holographic self-consistency:

$$M_P^2 \;=\; \frac{24\pi\,\alpha^2\,\Lambda_{\text{QCD}}^3}{H_0\,\Omega_\Lambda}, \tag{22}$$

yielding $M_P^{\text{pred}} = 1.2217 \times 10^{19}$ GeV versus experiment 1.2209×10^{19} GeV (**0.07% error**).

The vacuum energy density is

$$\rho_\Lambda \;=\; 9\alpha^2\,\Lambda_{\text{QCD}}^3\,H_0 \;=\; 2.52 \times 10^{-47}\ \text{GeV}^4, \tag{23}$$

matching the observed value exactly and resolving the 121-order-of-magnitude cosmological constant problem: most of the vacuum's information-theoretic energy is self-screened and does not gravitate.

The 4.8.8 tiling has zero Euler characteristic ($\chi = V - E + F = 0$), covering only flat 2-manifolds, making spatial flatness ($\Omega_k = 0$) topologically inevitable.

11 Grand Unification and the Hierarchy Problem (Parts 18–19)

11.1 The Feshbach Mechanism and the Colour Firewall (Part 18)

The Standard Model mass-generation mechanism emerges from the Feshbach projection through the R4-forbidden ν_R channel. Three structural theorems are established:

1. **Colour Firewall:** No path of any length within the R1+R2+R3-valid code space connects any quark to ν_R. Quarks and leptons acquire mass by topologically distinct mechanisms.

2. **Golden → Silver Ratio:** The Feshbach projection converts the lepton block's characteristic polynomial from the golden ratio ($x^2 - x - 1 = 0$) to the silver ratio ($x^2 - 2x - 1 = 0$), the fundamental eigenvalue of the 4.8.8 octagon.

3. **Hierarchy Problem Dissolved:** The fundamental quark–Higgs coupling is suppressed by $\sim 10^{-26}$ behind the colour firewall, giving one-loop Higgs mass corrections $\Delta m_H^2 \sim 10^{-16}\ \text{GeV}^2 \ll (125\ \text{GeV})^2$.

11.2 The Pati–Salam Identification (Part 19)

The four parity-check rules are identified as the exact $\mathbb{F}_2$ binary generators of the Pati–Salam GUT ($\mathrm{SU}(4)_C \times \mathrm{SU}(2)_L \times \mathrm{SU}(2)_R$):

Rule	**Breaking**	**Physical scale**	**Energy**
R1	4th generation	Cosmological boundary	$\sim M_P$
R3	$\mathrm{SU}(4)_C \to \mathrm{SU}(3)_C \times \mathrm{U}(1)_{B-L}$	Leptoquarks X/Y	$\sim 10^{15}$ GeV
R2	$\mathrm{SU}(2)_R$ breaking	$W_R^{\pm}$	$\sim 10^{15}$ GeV
R4	ν_R exclusion	Electroweak	246 GeV

The Topological Seesaw mechanism independently yields the R2 energy scale at $\sim 10^{15}$ GeV, confirming convergence with the GUT scale.

12 Comparison with the Standard Model

The table below summarises the key differences between the Standard Model and the Holographic Circlette framework.

Feature	**Standard Model**	**Holographic Circlette**
Free parameters	19–26 fitted to experiment	0–1 (only Λ_{QCD})
Fermion spectrum	Assumed (3 generations)	Derived (R1 constraint)
$\sin^2\theta_W$	Fitted	$= 2/9$ (derived)
Lepton masses	Yukawa couplings (fitted)	Koide formula ($\delta = 2/9$)
CKM matrix	4 parameters fitted	Derived from quantum walk
Strong CP problem	Unsolved (θ_{QCD} arbitrary)	No continuous θ vacuum (see text)
Gravity	Separate theory (GR)	Emerges as Fisher curvature
Dark energy	Λ fitted	$w_0 = -3/4$ (derived)
Hierarchy problem	Unresolved	Dissolved (10^{-26} suppression)
α	Measured	Derived to 3 ppb
ρ meson mass	Not predicted	$\sqrt{2}\,\varphi\,\Lambda_{\mathrm{QCD}}$ (derived, -2.0%)
Cosmological constant	10^{121} discrepancy	Resolved (self-screening)

Remark on the Strong CP problem. In standard QFT, the Strong CP phase θ is a continuous free parameter. Because the 4.8.8 framework replaces the continuous gauge vacuum with a discrete topological lattice governed by real, diagonal Laplacian eigenvalues, it natively lacks the continuous winding degeneracy required to support a non-zero θ_{QCD}. However, a formal proof of dynamic CP conservation in the emergent continuous limit remains an open topological problem.

13 Verifiable Claims

The following claims can be verified by independent calculation from the stated premises (the 8-bit code and the CNOT gate on the 4.8.8 lattice). Each claim is either a mathematical theorem or a numerical prediction testable against known experimental data.

1. Four Boolean parity-check rules on an 8-bit register select exactly 45 valid codewords corresponding to the Standard Model fermion spectrum.
2. The generalised Koide formula with $R = \sqrt{2}$, $\delta = 2/9$ reproduces m_e, m_μ, m_τ to 0.007%.
3. The partition $9 = 7 + 2$ yields $\sin^2\theta_W = 2/9$ (0.3% from experiment).
4. The W/Z mass ratio $M_W/M_Z = \sqrt{7/9} \approx 0.8819$ holds to 0.05%.
5. The XOR composite of all particles in beta decay vanishes identically, sector by sector.
6. The W^- boson is the literal XOR differential $d_L \oplus u_L = \texttt{00000100}$.
7. All six Standard Model gauge anomalies cancel exactly over the 45 Boolean codewords.
8. The discrete quantum walk on the 4.8.8 lattice reproduces single- and double-slit diffraction.
9. The loop-level walk operator projected onto the quark subspace reproduces Wolfenstein power counting $(\lambda, \lambda^2, \lambda^3)$ in the CKM matrix.
10. The bare Cabibbo angle $|V_{us}| \approx 0.237$ follows from the walk operator without continuous fitting.
11. The neutrino Koide parameters $R_\nu = 1$, $\delta_\nu = 1/3$ follow from CNOT inactivity for the $\mathrm{LQ} = 0$ sector.
12. The mass-squared ratio $\Delta m^2_{21}/\Delta m^2_{31}$ matches NuFIT 5.3 to 1.6%.
13. Near-maximal solar mixing ($\theta_{12} \approx 43.7°$) emerges at zeroth order from the lepton projection.
14. No path within the valid code space connects any quark to ν_R (Colour Firewall Theorem).
15. The Feshbach projection converts the golden ratio eigenvalue to the silver ratio (the C_8 octagon eigenvalue).
16. The Landauer bit-weight $w = \alpha\,\Lambda_{\mathrm{QCD}} \approx 2.42$ MeV predicts $m_d - m_u$ to 4% of FLAG 2024.
17. The nucleon mass $M_0 = 2\sqrt{2}\,\Lambda_{\mathrm{QCD}} \approx 939$ MeV follows from spectral graph theory of C_8.
18. The baryon octet mass splittings follow from $A = -7w/8$, $B = 4w$.
19. The bare fine-structure constant $\alpha_0 = 1/137$ follows from 136 confined microstates plus 1 emission pathway.
20. The discrete Dyson–Schwinger equation yields $\alpha^{-1} \approx 137.035\,999\,077$ (3 ppb accuracy).
21. The connected 4-point trace evaluates to -240, matching the E_8 root system.

22. $f_\pi = \Lambda_{\text{QCD}}/\sqrt{4\pi} \approx 93.66$ MeV (0.7% error).

23. The screened pion mass $m_\pi \approx 136.1$ MeV (1% of m_{π^0}).

24. The pion electromagnetic splitting $\Delta m = 4.56$ MeV reproduces Dashen's Theorem.

25. Dark energy $w_0 = -3/4$ from code-rule counting.

26. $M_P = 1.2217 \times 10^{19}$ GeV from holographic self-consistency (0.07% error).

27. Vacuum energy density $\rho_\Lambda = 9\alpha^2 \Lambda_{\text{QCD}}^3 H_0$ matches observation exactly.

Claims 28–32: Vector mesons and chiral consistency (Part 21):

28. The line graph of the meson flux-tube path gives $L(P_5) = P_4$ with leading eigenvalue $\varphi = (1+\sqrt{5})/2$ (Line Graph Theorem).

29. The $J^{PC} = 1^{--}$ quantum numbers force antipodal quark placement at $d = 4$ edges on C_8 (Antinode Theorem).

30. The bare ρ meson mass $m_\rho^{\text{bare}} = \sqrt{2}\,\varphi\,\Lambda_{\text{QCD}} \approx 760$ MeV (-2.0% from physical peak; matches quenched lattice QCD).

31. The tree-level decay width $\Gamma_\rho = (\varphi^2/12)\, m_\rho\, (1 - 4m_\pi^2/m_\rho^2)^{3/2} \approx 137$ MeV (-7.9% from experiment).

32. The KSFR low-energy theorem $m_\rho^2 = 2 f_\pi^2 g_{\rho\pi\pi}^2$ is satisfied identically by the framework values (chiral consistency).

Working results 33–40: Continuous-discrete interface (unpublished, 8 locked theorems):

33. The $k = 1$ and $k = 3$ harmonics on C_8 have identical magnitudes at every vertex (Phase Theorem).

34. The k-th harmonic on C_N is the Chebyshev polynomial T_k of the fundamental (Chebyshev Theorem).

35. Coherent transmission $\times$ Laplacian eigenvalue $= 1$ for every harmonic: $T_k \cdot \lambda_k = 1$ (Bridge-Tension Duality).

36. The ratio of coherent transmission to coherent input on the C_4 bridge is flavour-independent: $T/I = 1/(E-1)$ (Universal Transmission Law).

37. Pion and kaon projection coefficients onto the C_4 eigenmodes $\lambda = \pm 2$ are exactly swapped (Spectral Swap).

38. The hybrid form factor factorises as $|M_1|^2 \propto [\sqrt{2} + \cos(qa)]$ (pion) and $|M_3|^2 \propto [\sqrt{2} - \cos(qa)]$ (kaon), with the modulation factors exhibiting exact complementarity: $[\sqrt{2} + \cos(qa)] + [\sqrt{2} - \cos(qa)] = 2\sqrt{2}$ for all q.

39. The pion and kaon spectral bands are non-overlapping, with edges at powers of the silver ratio $\delta_S = 1 + \sqrt{2}$ (Silver Ratio Band Structure).

40. The spectral gap between the pion and kaon bands is exactly $\sqrt{2}$—the C_8 adjacency eigenvalue ($\sqrt{2}$ Band Gap).

14 Testable Predictions

The following predictions are accessible to current or planned experiments and would, if confirmed, provide strong evidence for the framework; if falsified, they would rule it out.

1. **Normal neutrino mass ordering.** JUNO is projected to determine this at 3σ within its first 6 years of operation.

2. **Lightest neutrino mass $m_1 \approx 0.8$ meV.** Below current KATRIN sensitivity but within reach of Project 8.

3. **Neutrino mass sum $\Sigma m_i \approx 60$ meV.** CMB-S4 combined with DESI is projected to reach ~ 30 meV sensitivity.

4. **Neutrino Koide ratio $Q_\nu = 1/2$.** A sharp discriminator between mass models, testable as oscillation data improves.

5. **Majorana neutrino.** Neutrinoless double-beta decay predicted, with effective Majorana mass $|m_{ee}| \approx 3.7$ meV. Testable by LEGEND-1000, nEXO, and CUPID.

6. **Dark energy equation of state $w_0 = -3/4$ and $w_a = -1/4$.** DESI DR2 already shows $w_0 = -0.752 \pm 0.071$. The full CPL trajectory $w(a) = -1 + a/4$ will be tested by Euclid and the Vera Rubin Observatory.

7. **Proton stability.** Proton stability is mathematically guaranteed at the Standard Model scale because the weak interaction (the CNOT gate) is topologically incapable of flipping its own control bit (Part 2). Absolute stability is preserved within the unperturbed code space; macroscopic baryon decay can only occur via non-perturbative GUT-scale topological defect transitions (Part 19), the exact rate of which remains an open calculation. Hyper-Kamiokande will probe $\tau_p \sim 10^{35}$ years.

8. **Spatial flatness $\Omega_k = 0$ exactly.** The 4.8.8 tiling has zero Euler characteristic, requiring a flat manifold.

9. **The $t\bar{t}H$ Yukawa coupling does not run logarithmically** as predicted by the Standard Model. The Feshbach mechanism sets the coupling non-perturbatively. Testable at $\sim 1\%$ precision at future e^+e^- Higgs factories (ILC, FCC-ee, CEPC).

10. **No fourth generation of fermions.** The R1 constraint ($G_0 \cdot G_1 \neq 1$) structurally forbids it.

11. **Planck mass formula consistency.** As lattice QCD precision on Λ_{QCD} improves beyond 0.1%, the relation $M_P^2 = 24\pi\alpha^2\Lambda_{\text{QCD}}^3/(H_0\Omega_\Lambda)$ must hold simultaneously. Failure at that precision falsifies the framework.

12. **Hadronic form factor intermediate-window deviations.** At the continuous-discrete interface, the $k = 3$ strange quark phase geometrically forces a discrete Chebyshev momentum modulation ($\propto \cos(qa)$). This mathematically precludes a globally smooth VMD monopole form factor, providing a parameter-free geometric mechanism for the intermediate-window deviations observed in hadronic form factors (working results, Section 9).

13. **The ρ meson mass-to-width ratio is fixed by the golden ratio.** As NLO lattice QCD and dispersive analyses improve, the bare ρ mass must converge to $m_\rho^{\text{bare}} = \sqrt{2}\,\varphi\,\Lambda_{\text{QCD}} = 760 \pm 2$ MeV, and the tree-level coupling must satisfy $g_{\rho\pi\pi} = 2\varphi\sqrt{\pi}$.

15 Conclusion

The Holographic Circlette framework, developed across twenty-one papers, demonstrates that a remarkably broad spectrum of fundamental physics—from charged lepton masses to the cosmological constant to the vector meson sector—can be derived from a single discrete structure: an 8-bit quantum error-correcting code on a 4.8.8 Archimedean lattice with a CNOT update rule.

The framework's principal strength is its economy: where the Standard Model requires 19–26 fitted parameters, the circlette uses zero or one (the QCD scale Λ_{QCD}, which sets the overall energy scale). Every other quantity is derived from the topology of the lattice and the algebra of the error-correcting code.

The thirteen testable predictions listed in Section 14 span particle physics, cosmology, and gravitational physics. Several are accessible to experiments currently in operation or under construction. The framework is therefore not merely a repackaging of known results, but a genuinely falsifiable theory.

Whether or not every prediction survives experimental scrutiny, the programme demonstrates that the "unreasonable effectiveness" of mathematics in physics may have a surprisingly concrete origin: the laws of nature as the error-correction protocols of a discrete computational substrate.

References

[1] D. G. Elliman, "The Holographic Circlette: Part I—The Encoding and Its Dynamics," Neuro-Symbolic Ltd, Preprint (2026).

[2] D. G. Elliman, "The Holographic Circlette: Part II—Composites, Decays, and the Zero-Sum Identity," Neuro-Symbolic Ltd, Preprint (2026).

[3] D. G. Elliman, "The Double-Slit Experiment on a Discrete Holographic Lattice," Neuro-Symbolic Ltd, Preprint (2026).

[4] D. G. Elliman, "Topological Origin of the Quark Mixing Hierarchy and CP Violation in a Discrete Information Space," Zenodo, doi:10.5281/zenodo.18763144 (2026).

[5] D. G. Elliman, "The Holographic Circlette: Part V—Neutrino Masses from the Lattice Koide Formula," Neuro-Symbolic Ltd, Preprint (2026).

[6] D. G. Elliman, "The Holographic Circlette: Part VI—Topological Origin of Large Lepton Mixing and the PMNS Matrix," Neuro-Symbolic Ltd, Preprint (2026).

[7] D. G. Elliman, "The Holographic Circlette: Part VII—Exact Standard Model Gauge Anomaly Cancellation from Discrete Boolean Constraints," Neuro-Symbolic Ltd, Preprint (2026).

[8] D. G. Elliman, "The Holographic Circlette: Part VIII—Hadron Topology, the Meson-Lepton Homomorphism, and the Geometric Origin of B_s Mixing," Neuro-Symbolic Ltd, Preprint (2026).

[9] D. G. Elliman, "The Holographic Circlette: Part IX—Topological Isolation of the Electron and the Factorisation of the PMNS Matrix," Neuro-Symbolic Ltd, Preprint (2026).

[10] D. G. Elliman, "The Holographic Circlette: Part X—Algorithmic Inertia, Landauer Bit-Weight, and the Topological Origin of the Proton-Neutron Mass Difference," Neuro-Symbolic Ltd, Preprint (2026).

[11] D. G. Elliman, "The Holographic Circlette: Part XI—Spectral Graph Energy, Absolute Nucleon Mass, and the Parameter-Free Baryon Octet," Neuro-Symbolic Ltd, Preprint (2026).

[12] D. G. Elliman, "The Holographic Circlette: Part XII—Topological Origin of the Fine-Structure Constant and Discrete Vacuum Polarization," Neuro-Symbolic Ltd, Preprint (2026).

[13] D. G. Elliman, "The Holographic Circlette: Part XIII—Chiral Symmetry Breaking and the Pion Mass from Discrete Topological Screening," Neuro-Symbolic Ltd, Preprint (2026).

[14] D. G. Elliman, "The Holographic Circlette: Part XIV—Electromagnetic Dipole Radiation and Isospin Breaking in the Meson Sector," Neuro-Symbolic Ltd, Preprint (2026).

[15] D. G. Elliman, "The Holographic Circlette: Part XV—The Rosetta Stone: How 3D Geometry Emerges from a Discrete Lattice," Neuro-Symbolic Ltd, Preprint (2026).

[16] D. G. Elliman, "The Holographic Circlette: Part XVI—The DESI Anomaly and the Lattice Equation of State," Neuro-Symbolic Ltd, Preprint (2026).

[17] D. G. Elliman, "The Holographic Circlette: Part XVII—Topological Thawing and the Exact Geometric Derivation of the Dark Energy Trajectory w_a," Neuro-Symbolic Ltd, Preprint (2026).

[18] D. G. Elliman, "The Holographic Circlette: Part XVIII—The Feshbach Mechanism, the Colour Firewall, and the Pati-Salam Identification," Neuro-Symbolic Ltd, Preprint (2026).

[19] D. G. Elliman, "The Holographic Circlette: Part XIX—The $\mathbb{F}_2$ Pati-Salam Isomorphism and the Cosmological Cooling of the Error-Correcting Vacuum," Neuro-Symbolic Ltd, Preprint (2026).

[20] D. G. Elliman, "The Holographic Circlette: Part XX—Newton's Constant from Holographic Self-Consistency of the 4.8.8 Lattice," Neuro-Symbolic Ltd, Preprint (2026).

[21] D. G. Elliman, "The Holographic Circlette: Part XXI—Vector Mesons, Line Graph Topology, and Chiral Consistency on the 4.8.8 Lattice," Neuro-Symbolic Ltd, Preprint (2026).

[22] Particle Data Group, "Review of Particle Physics," Phys. Rev. D **110**, 030001 (2024).

[23] I. Esteban et al., "NuFIT 5.3," http://www.nu-fit.org (2024).

[24] FLAG Working Group, "FLAG Review 2024," Eur. Phys. J. C (2024).

[25] DESI Collaboration, "DESI DR2 Results," arXiv:2503.14738 (2025).